IEEE Access
Multidisciplinary ⋮ Rapid Review ⋮ Open Access Journal

Received December 29, 2019, accepted January 12, 2020, date of publication January 17, 2020, date of current version February 6, 2020.

Digital Object Identifier 10.1109/ACCESS.2020.2967153

Resource Allocation in NOMA-Enhanced Full-Duplex Symbiotic Radio Networks

YATING LIAO[1,2], GANG YANG[1,2], (Member, IEEE), AND YING-CHANG LIANG[2], (Fellow, IEEE)

[1]National Key Laboratory of Science and Technology on Communications, University of Electronic Science and Technology of China, Chengdu 611731, China
[2]Center for Intelligent Networking and Communications (CINC), University of Electronic Science and Technology of China, Chengdu 611731, China

Corresponding author: Gang Yang (yanggang@uestc.edu.cn)

This work was supported in part by the National Natural Science Foundation of China Grant 61631005, Grant U1801261, and Grant 61601100, the National Key Research and Development Program of China under Grant 2018YFB1801105, and in part by the 111 Project under Grant B20064.

ABSTRACT This paper studies a full-duplex symbiotic radio network, where a full-duplex access point (FAP) transmits downlink orthogonal frequency division multiplexing signals to a legacy user (LU) and simultaneously receives signals backscattered from multiple passive backscatter devices (BDs) with capability of radio-frequency energy harvesting. A non-orthogonal-multiple-access enhanced dynamic-time-division-multiple-access (NOMA-DTDMA) transmission scheme is proposed to exploit the channel dynamics and further improve the spectrum efficiency. In order to maximize the throughput performance and ensure BD fairness, we maximize the minimum throughput among all BDs by jointly optimizing the FAP's subcarrier power allocation, the BDs' backscatter time allocation and power reflection coefficients, subject to the LU's throughput requirement, the BDs' harvested energy requirements, and other practical constraints. An efficient iterative algorithm is proposed to solve the formulated non-convex problem, by utilizing the block coordinated descent and successive convex optimization techniques. The convergence and complexity of the proposed algorithm are also analyzed. Numerical results show that the proposed NOMA-DTDMA scheme significantly outperforms the benchmark scheme of dynamic TDMA in terms of both throughput performance and BD fairness. Also, the trade-off performances between the BDs' throughput and the LU's throughput requirement as well as the BDs' harvested energy requirements are numerically verified.

INDEX TERMS Full-duplex symbiotic radio network, iterative algorithm, joint resource allocation, non-orthogonal-multiple-access (NOMA), throughput optimization.

I. INTRODUCTION

Internet-of-Things (IoT) which supports the interconnection of massive wireless devices, is an important application scenario of the fifth-generation (5G) and future wireless communication systems [1]–[3]. Massive IoT connections require huge spectrum and energy resources [4]. Backscatter communication, which enables passive backscatter devices (BDs) to modulate their information over incident sinusoidal carriers or ambient radio-frequency (RF) carriers without using costly and power-hungry RF transmitter [5]–[9], is widely used in certain IoT systems like radio frequency identification (RFID). Recently, a new symbiotic radio (SR) paradigm was proposed in [10]–[12], which enables passive IoT devices to backscatter information by sharing the spectrum and infrastructure (e.g., transmitter, receiver) of existing wireless communication systems. Hence, SR is a promising spectrum- and energy-efficient as well as cost-efficient communication technology for future IoT.

Recently, SR has attracted growing research interests [10]–[15]. In [10], it was shown that the signal from the BD in an SR system can be exploited as additional multipath to achieve bit-error-rate performance improvement. In [11], the transmit beamforming was optimized for an SR system in fading channels, and the weighted sum rate of the primary transmission and backscatter transmission is maximized. In [14], full-duplex technique was introduced into an SR system, which enables a BD to transmit and receive information simultaneously. In [15], the authors derived the closed-form expressions of the outage probabilities and the ergodic rate for a system integrating non-orthogonal-multiple-access (NOMA) into SR.

The associate editor coordinating the review of this manuscript and approving it for publication was Yan Huo.

On the other hand, NOMA, which transmits (receives) signals to (from) multiple users in the same radio resource, is recognized as an important candidate for future wireless communication systems, due to its appearing advantages such as enhanced spectrum efficiency and support for massive connections [16]–[18]. Specifically, in power-domain NOMA systems, multiple users share the same time-frequency resource block by superposing the messages in power domain [19], and the receiver adopts the successive interference cancellation technique to cancel inter-user interference within the same cell [20], [21]. The optimal user pairing schemes for uplink and downlink NOMA were studied in [22] and [23], respectively. The time and power resource allocation was optimized in [24] for a NOMA-enhanced wireless powered communication network. The millimeter-wave communication with NOMA was studied in [25], and the system's sum rate was maximized. Recently, a NOMA-enhanced monostatic backscatter communication system with co-located carrier transmitter and backscatter receiver was studied in [26], where the outage probability and average number of successfully decoded bits were analyzed. In [27], the throughput performance is optimized for a NOMA-enhanced bistatic backscatter communication network.

A full-duplex symbiotic radio network (FSRN) was proposed in [28], in which a full-duplex access point (FAP) transmits downlink orthogonal frequency division multiplexing (OFDM) signals to a legacy user (LU) and simultaneously receives signals backscattered from multiple BDs in a time-division-multiple-access (TDMA) manner. In practice, such an FSRN integrates IoT transmission into existing wireless communication systems, and typical application scenarios include smart wearable network, smart home, etc. However, for such TDMA-based FSRN, the throughput of each BD decreases as the number of BDs increases. To further enhance its spectrum efficiency, we exploit NOMA for the BDs' uplink transmission in an FSRN, which has not been studied in the literature to our best of knowledge.

This paper considers a NOMA-enhanced FSRN over OFDM carriers as shown in Fig. 1, which consists of an FAP, an LU and multiple passive BDs. The FAP transmits downlink OFDM signals to the LU and simultaneously receives signals backscattered from BDs via a hybrid scheme of NOMA and dynamic TDMA (NOMA-DTDMA). The BDs can also harvest energy from their incident OFDM signals. The main contributions of this paper are summarized as follows:

- First, a NOMA-DTDMA scheme is proposed for an FSRN to improve its spectrum efficiency and exploit the channel dynamics. The throughput performance of the proposed NOMA-DTDMA scheme is analyzed, for both cases that the FAP detects BDs' signals based on maximum-ratio-combining (MRC) and equal-gain-combining (EGC), respectively.
- Second, in order to optimize the throughput performance and ensure BD fairness, we formulate a problem to maximize the minimum throughput among all BDs, by jointly optimizing the FAP's subcarrier power allocation, the BDs' backscatter time and power reflection coefficients, subject to the FAP's total-power and peak-power constraints, the LU's throughput requirement, the BDs' harvested energy requirements and backscatter-time constraints. This problem optimizes the throughput performance of a NOMA-enhanced FSRN from multiple design dimensions. It is non-convex due to coupled variables and complicated constraint functions, and thus difficult to be solved optimally.
- Third, an efficient iterative algorithm is proposed to obtain a suboptimal solution of the formulated non-convex problem, by utilizing the block coordinated descent (BCD) and successive convex optimization (SCO) techniques. The convergence and complexity of the proposed algorithm are also analyzed.
- Finally, numerical results show that the proposed NOMA-DTDMA scheme for an FSRN significantly outperforms the benchmark scheme of dynamic TDMA in terms of both throughput performance and BD fairness. Moreover, the tradeoff performances between the BDs' throughput and the LU's throughput requirement as well as the BDs' harvested energy requirements are validated.

The rest of this paper is organized as follows. Section II presents the system model for a NOMA-DTDMA based FSRN over ambient OFDM carriers. Section III formulates the minimum-throughput maximization problem. Section IV proposes an efficient iterative algorithm based on the BCD and SCO techniques. Section V provides the numerical results. Finally, Section VI concludes this paper.

II. SYSTEM MODEL

As shown in Fig. 1, we consider an FSRN consisting of an FAP with two antennas for transmitting and receiving, respectively, an LU, and U ($U \geq 1$) BDs each equipped with a single antenna. The FAP transmits downlink OFDM signals to the LU and simultaneously receives the uplink signals backscattered from the BDs. The BDs modulate their information over the incident OFDM carriers by intentionally switching their antenna impedances [29]. Also, the BD can harvest RF-energy from the incident signals to provide sufficient energy for their own operation.

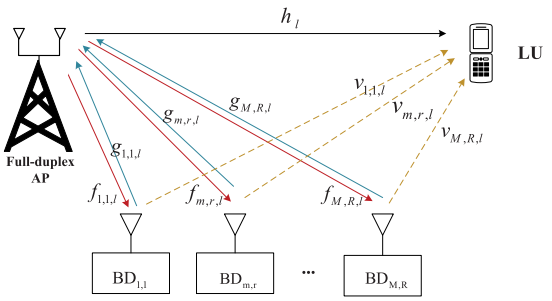

FIGURE 1. System description for an FSRN.

A framed-based transmission scheme is proposed in this paper, which is an integration of NOMA and dynamic TDMA. For notational simplicity, we assume that the number of BDs $U = MR$ with $M \geq 1$ and $R \geq 1$, and R BDs perform NOMA multiplexing to the FAP in the m-th transmission slot, for $m = 1, \ldots, M$. In practice, the BDs can be grouped by using the following method. In the first training phase consisting of MR training slots. The FAP transmits constant training signal to all BDs, and only one BD backscatters incident signal with the same (fixed) power reflection coefficient in its assigned training slot, with all other BDs keeping silent. For a typical FSRN application example like smart home, tens of BDs are deployed near the FAP with average distance of tens of meters, and are static or moving slowly. The FAP-BD-FAP propagation time is on the level of tens of nanoseconds. The whole training phase is much shorter than the typical coherence time of about several milliseconds.

Without loss of generality, the BDs with index from 1 to MR are indexed in an decreasing order according to their receiving power levels. The FAP categorizes all BDs into R groups, and the r-th group consists of the BDs with indexes from $((r-1)M+1)$ to rM. In the second transmission phase consisting of M transmission slots, the FAP schedules the BD with index $((r-1)M+m)$ (i.e., denoted as BD (m, r) in the sequel) from the r-th energy group, for $r = 1, \ldots, R$, to access the FAP in a NOMA manner. The time duration of data transmission is normalized to one second for notational simplicity. Denote the time duration of the m-th transmission slot by τ_m, $0 \leq \tau_m \leq 1$, subject to the normalization constraint $\sum_{m=1}^{M} \tau_m = 1$. Denote the BDs' backscatter time vector $\boldsymbol{\tau} = [\tau_1, \ldots, \tau_M]^T \in \mathcal{R}^M$.

We consider the block flat-fading channel model, and assume that the channel block length is much longer than the OFDM symbol period. As shown in Fig. 1, denote the L_{h}-path legacy channel response from the FAP to the LU by h_l, the L_{f}-path forward channel response from the FAP to the (m, r)-th BD by $f_{m,r,l}$, the L_{v}-path interference channel response from the (m, r)-th BD to the LU by $v_{m,r,l}$, and the L_{g}-path backward channel response from the (m, r)-th BD to the FAP by $g_{m,r,l}$. The number of subcarriers of the transmitted OFDM signals is denoted by N ($N \geq 1$). For the forward channel from the FAP to the (m, r)-th BD, the frequency response at the k-th subcarrier is defined as $F_{m,r,k} = \sum_{l=0}^{L_{\mathsf{f}}-1} f_{m,r,l} e^{\frac{-j2\pi kl}{N}}$, for $k = 0, \ldots, N-1$. Similarly, $G_{m,r,k} = \sum_{l=0}^{L_{\mathsf{g}}-1} g_{m,r,l} e^{\frac{-j2\pi kl}{N}}$, $V_{m,r,k} = \sum_{l=0}^{L_{\mathsf{v}}-1} v_{m,r,l} e^{\frac{-j2\pi kl}{N}}$, and $H_k = \sum_{l=0}^{L_{\mathsf{h}}-1} h_l e^{\frac{-j2\pi kl}{N}}$.

Denote the FAP's transmitted information symbol at the k-th subcarrier in the n-th OFDM symbol period of the m-th (transmission) slot by $S_{m,k}(n) \in \mathcal{C}$, with $\mathcal{C}$ denoting the complex number set, which is assumed to follow the circularly symmetric complex Gaussian (CSCG) distribution with zero mean and unit variance, i.e., $S_{m,k}(n) \sim \mathcal{CN}(0, 1)$. After performing inverse discrete Fourier transform (IDFT) at the FAP, a cyclic prefix (CP) of length N_{cp} is added at the beginning of each OFDM symbol. In each OFDM symbol period, the transmitted time-domain signal is

$$s_{m,t}(n) = \frac{1}{N} \sum_{k=0}^{N-1} \sqrt{P_{m,k}} S_{m,k}(n) e^{\frac{j2\pi kt}{N}}, \tag{1}$$

where $t = 0, 1, \ldots, N-1$, $P_{m,k}$ denotes the allocated power at the k-th subcarrier in the m-th slot. $\mathbf{P} = [\mathbf{p}_1\ \mathbf{p}_2\ \ldots\ \mathbf{p}_M] \in \mathcal{R}^{N \times M}$ denotes the subcarrier power allocation matrix, with the power allocation vector $\mathbf{p}_m = [P_{m,0}, \ldots, P_{m,N-1}]^T$ and $\mathcal{R}$ denoting the real number set.

In the m-th slot, the incident signal of the (m, r)-th BD can be written as $s_{m,t}(n) \otimes f_{m,r,l}$, with $\otimes$ denoting the convolution operator. For the (m, r)-th BD, a proportion $\alpha_{m,r}$ of the incident power is reflected, while the remaining power with proportion $(1 - \alpha_{m,r})$ propagates to the energy-harvesting circuit.[1] As a common assumption in the RF-based wireless power transfer literature [31]–[35], we assume that the harvested power is linearly proportional[2] to the received power and the noise power cannot be harvested. Denote power reflection coefficient vector $\boldsymbol{\alpha} = [\alpha_{1,1} \ldots \alpha_{1,R}, \ldots, \alpha_{M,1} \ldots \alpha_{M,R}]^T \in \mathcal{R}^{MR}$ (with $0 \leq \alpha_{m,r} \leq 1$). Denote the energy-harvesting efficiency constant of the (m, r)-th BD by $\eta_{m,r}$ ($0 \leq \eta_{m,r} \leq 1$). The total energy harvested by the (m, r)-th BD is given by

$$E_{m,r} = \eta_{m,r} \sum_{k=0}^{N-1} |F_{m,r,k}|^2 \Big[\tau_m P_{m,k} (1 - \alpha_{m,r}) + \ldots \sum_{i=1,\ i \neq m}^{M} \tau_i P_{i,k} \Big]. \tag{2}$$

Let $X_{m,r} \sim \mathcal{CN}(0, 1)$ denote the transmitted signal of the (m, r)-th BD in the n-th OFDM symbol period, whose duration is assumed to be the same as the OFDM symbol period. The received time-domain signal backscattered in m-th slot is given by

$$y_{m,t}(n) = \sqrt{P_{m,k}} \cdot \sum_{r=1}^{R} \sqrt{\alpha_{m,r}} s_{m,t}(n) \otimes f_{m,r,l} \otimes g_{m,r,l} X_{m,r}(n) + w_{m,t}(n), \tag{3}$$

where $w_{m,t}(n)$ denotes the additive white Gaussian noise (AWGN) with power σ^2, i.e., $w_{m,t}(n) \sim \mathcal{CN}(0, \sigma^2)$.

After removing CP and performing discrete Fourier transform (DFT) at the FAP, the received frequency-domain signal in the m-th slot is given by

$$Y_{m,k}(n) = \sqrt{P_{m,k}} \cdot \sum_{r=1}^{R} \sqrt{\alpha_{m,r}} S_{m,k}(n) F_{m,r,k} G_{m,r,k} X_{m,r}(n) + W_{m,k}(n), \tag{4}$$

where $W_{m,k}(n) \sim \mathcal{CN}(0, \sigma^2)$.

[1] Energy harvesting can prolong IoT devices' service life by extracting energy from the external natural environment. The possibility of powering IoT devices by using ambient RF sources like TV and cellular signals has been demonstrated [30].

[2] The linear energy-harvesting model is adopted for analytical tractability and performance optimization in this paper, although some non-linear models are also available [34].

According to the demodulation rule in uplink NOMA, the FAP decodes the signals from BDs with indexes from group 1 to group R. We assume that the FAP detects the BD symbols $X_{m,r}(n)$'s based on MRC or EGC [36]. When the FAP adopts MRC detector $\omega^1_{m,r,k} = \frac{\sqrt{P_{m,k}\alpha_{m,r}}F^*_{m,r,k}G^*_{m,r,k}}{||\sum_{k=0}^{N-1} P_{m,k}\alpha_{m,r}|F_{m,r,k}G_{m,r,k}|^2||}$ to decode signals from the k-th subcarrier of the (m, r)-th BD, the corresponding signal-to-interference-plus-noise ratio (SINR) of the (m, r)-th BD is

$$\gamma^1_{m,r} = \begin{cases} \dfrac{\alpha_{m,r}}{\theta(\mathbf{p},\alpha)+\sigma^2}\displaystyle\sum_{k=0}^{N-1} P_{m,k}A_{m,r,k}, & 1 \le r \le R-1 \\ \dfrac{\alpha_{m,R}}{\sigma^2}\displaystyle\sum_{k=0}^{N-1} P_{m,k}A_{m,R,k}, & r = R \end{cases} \tag{5}$$

where $A_{m,r,k} = |F_{m,r,k}G_{m,r,k}|^2$, and $\theta(\mathbf{p},\alpha) = \frac{\sum_{k=0}^{N-1} P_{m,k}\alpha_{m,r}A_{m,r,k}\sum_{i=r+1}^{R} P_{m,k}\alpha_{m,i}A_{m,i,k}}{\sum_{k=0}^{N-1} P_{m,k}\alpha_{m,r}A_{m,r,k}}$ represents the interference from other BDs. Note that there is no interference when $r = R$ since other BDs' signals have been decoded successfully.

When the FAP adopts EGC detector $\omega^2_{m,r,k} = \frac{F_{m,r,k}G_{m,r,k}}{|F_{m,r,k}G_{m,r,k}|}$ to decode signals from the k-th subcarrier of the (m, r)-th BD, the corresponding SINR of the (m, r)-th BD is

$$\gamma^2_{m,r} = \begin{cases} \dfrac{\sum_{k=0}^{N-1} P_{m,k}\alpha_{m,r}A_{m,r,k}}{\sum_{k=0}^{N-1}\sum_{i=r+1}^{R} P_{m,k}\alpha_{m,i}A_{m,i,k}+N\sigma^2}, & 1 \le r \le R-1 \\ \dfrac{\alpha_{m,R}}{N\sigma^2}\displaystyle\sum_{k=0}^{N-1} P_{m,k}A_{m,R,k}, & r = R \end{cases} \tag{6}$$

where $\sum_{k=0}^{N-1}\sum_{i=r+1}^{R} P_{m,k}\alpha_{m,i}A_{m,i,k}$ represents the interference from other BDs. Similarly, there is no interference when $r = R$, since other BDs' signals have been decoded successfully. It is standard to prove that $\gamma^1_{m,r} > \gamma^2_{m,r}$ through some algebra operations.

Hence, the (m, r)-th BD's throughput is given by

$$R_{m,r}(\tau_m, \alpha_{m,r}, \mathbf{p}_m) = \frac{\tau_m}{N}\log\left(1+\gamma^i_{m,r}\right), \quad \forall i = 1, 2 \tag{7}$$

where $i = 1$ and $i = 2$ correspond to the cases where the FAP performs MRC and EGC, respectively.

The LU receives both the downlink legacy signal and the backscattered signals from BDs. Similar to (4), the received frequency-domain signal at the LU is given by

$$Z_{m,k}(n) = \sqrt{P_{m,k}}\sum_{r=1}^{R}\sqrt{\alpha_{m,r}}F_{m,r,k}V_{m,r,k}S_{m,k}(n)X_{(m,r)}(n) + \sqrt{P_{m,k}}H_kS_{m,k}(n) + \widetilde{W}_{m,k}(n), \quad \forall k, m \tag{8}$$

where $\widetilde{W}_{m,k}(n) \sim \mathcal{CN}(0, \sigma^2)$.

The signals backscattered from BDs are interferences, thus the throughput of the LU can be written as

$$\widetilde{R}(\boldsymbol{\tau}, \boldsymbol{\alpha}, \mathbf{P}) = \frac{1}{N}\sum_{m=1}^{M}\tau_m\sum_{k=0}^{N-1}\log\left(1+\frac{P_{m,k}|H_k|^2}{P_{m,k}\sum_{r=1}^{R}\alpha_{m,r}B_{m,r,k}+\sigma^2}\right), \tag{9}$$

where $B_{m,r,k} = |F_{m,r,k}V_{m,r,k}|^2$.

III. PROBLEM FORMULATION

In this section, in order to optimize the throughput performance and ensure BD fairness, we maximize the minimum throughput among all BDs, by jointly optimizing the FAP's subcarrier power allocation (i.e., $\mathbf{P}$), the BDs' backscatter time (i.e., $\boldsymbol{\tau}$) and power reflection coefficients (i.e., $\boldsymbol{\alpha}$). Mathematically, the problem is formulated as follows

$$\max_{Q,\boldsymbol{\tau},\boldsymbol{\alpha},\mathbf{P}} \quad Q \tag{10a}$$

$$\text{s.t. } \frac{\tau_m}{N}\log\left(1+\gamma^i_{m,r}\right) \ge Q, \quad \forall i, m, r \tag{10b}$$

$$\sum_{m=1}^{M}\frac{\tau_m}{N}\sum_{k=0}^{N-1}\log\left(1+\frac{P_{m,k}|H_k|^2}{P_{m,k}\sum_{r=1}^{R}\alpha_{m,r}B_{m,r,k}+\sigma^2}\right) \ge D \tag{10c}$$

$$\eta_{m,r}\sum_{k=0}^{N-1}|F_{m,r,k}|^2\Big[\tau_mP_{m,k}(1-\alpha_{m,r})+\sum_{i=1,\ i\neq m}^{M}\tau_iP_{i,k}\Big] \ge \bar{E}_{m,r}, \quad \forall m,\ r \tag{10d}$$

$$\sum_{m=1}^{M}\sum_{k=0}^{N-1}\tau_mP_{m,k} \le \bar{P} \tag{10e}$$

$$\sum_{m=1}^{M}\tau_m \le 1 \tag{10f}$$

$$\tau_m \ge 0, \quad \forall m \tag{10g}$$

$$0 \le P_{m,k} \le P_{\text{peak}}, \quad \forall m,\ k \tag{10h}$$

$$0 \le \alpha_{m,r} \le 1, \quad \forall m,\ r. \tag{10i}$$

Note that $i = 1$ and $i = 2$ in (10b) correspond to the cases where the FAP detects the BD signals based on MRC and EGC, respectively. (10b) is the throughput constraints for all BDs; (10c) is the required minimum throughput D constraint for LU; (10d) is the required minimum energy $\bar{E}_{m,r}$ constraint for BDs; (10e) is the maximum transmission-power $\bar{P}$ constraint for FAP; (10f) and (10g) are the normalization constraint and the non-negative constraint for each backscatter time, respectively; (10h) is the peak-power P_{peak} constraint and non-negative constraint for each subcarrier power; (10i) is the reflection coefficient constraint.

Problem (10) aims to optimize the throughput performance of an FSRN from multiple design dimensions. However, it is non-convex and thus difficult to be solved optimally.

The nonconvexity comes from the coupled optimization variables in (10b), (10c), (10d), and (10e), as well as the complicated constraint functions in (10b) and (10c).

IV. OPTIMAL SOLUTION

In this section, an efficient iterative algorithm is proposed to solve problem (10). Since problem (10) is not jointly convex with respect to the variables $\boldsymbol{\alpha}$ and $\mathbf{P}$, we utilize the BCD [37] (i.e., block coordinate descent) and SCO [38] (i.e., successive convex optimization) techniques to obtain a suboptimal solution. In the sequel, the superscript $\{j\}$ (with $j = 1, 2, \ldots$) in $\boldsymbol{\tau}$, $\boldsymbol{\alpha}$ and $\mathbf{P}$ to indicate their values in the j-th algorithmic iteration. After presenting the overall algorithm, its convergence and complexity are also analyzed.

A. SOLUTION FOR FSRN WITH MRC-BASED FAP

In this subsection, the case $i = 1$ in (10b) is considered, which means that the FAP detects the BD signals based on MRC.

1) BACKSCATTER TIME ALLOCATION OPTIMIZATION

In iteration $j, j \geq 1$, for given power reflection coefficient vector $\boldsymbol{\alpha}^{\{j\}}$ and subcarrier power allocation matrix $\mathbf{P}^{\{j\}}$, the backscatter time allocation vector $\boldsymbol{\tau}$ can be optimized by solving the following problem

$$\text{(P1-a)}: \max_{Q,\boldsymbol{\tau}} \quad Q \tag{11a}$$

$$\text{s.t. (10b), (10c), (10d), (10e), (10f), (10g).} \tag{11b}$$

Since problem (11) is a standard linear programming (LP), it can be solved efficiently by CVX [39].

2) REFLECTION POWER ALLOCATION OPTIMIZATION

For given backscatter time allocation vector $\boldsymbol{\tau}^{\{j\}}$ and subcarrier power allocation matrix $\mathbf{P}^{\{j\}}$, the power reflection coefficient vector $\boldsymbol{\alpha}$ can be optimized by solving

$$\text{(P1-b)}: \max_{Q,\boldsymbol{\alpha}} \quad Q \tag{12a}$$

$$\text{s.t. (10b), (10c), (10d), (10i).} \tag{12b}$$

Since the constraint function $\widetilde{R}_1(\boldsymbol{\alpha})|_{\boldsymbol{\tau}^{\{j\}},\mathbf{P}^{\{j\}}}$ in (10b) and $\widetilde{R}_2(\boldsymbol{\alpha})|_{\boldsymbol{\tau}^{\{j\}},\mathbf{P}^{\{j\}}}$ in (10c) are non-concave with respect to $\alpha_{m,r}$, problem (12) is non-convex. The constraint function $\widetilde{R}_1(\boldsymbol{\alpha})|_{\boldsymbol{\tau}^{\{j\}},\mathbf{P}^{\{j\}}}$ can be rewritten as follows

$$\widetilde{R}_1(\boldsymbol{\alpha})|_{\boldsymbol{\tau}^{\{j\}},\mathbf{P}^{\{j\}}} = \frac{\tau_m^{\{j\}}}{N}\Bigg[-\log\left(C_{m,r}\right) + \ldots \log\left(C_{m,r}+\Big(\sum_{k=0}^{N-1} P_{m,k}^{\{j\}}\alpha_{m,r}A_{m,r,k}\Big)^2\right)\Bigg], \quad 1 \leq r \leq R-1 \tag{13}$$

where we define $C_{m,r} \triangleq \sum_{k=0}^{N-1}[P_{m,k}^{\{j\}}\alpha_{m,r}A_{m,r,k} \times (\sum_{i=r+1}^{R} P_{m,k}^{\{j\}}\alpha_{m,i}A_{m,i,k} + \sigma^2)]$, for convenience of expression.

Since the constraint (10b) is in the form that the constraint function is greater than or equal to a certain value, this constraint is convex on condition that its constraint function is concave. However, the convex component (i.e., the first negative item in square brackets in (13)) makes the constraint function in (13) neither convex nor concave in general. Hence, the constraint (10b) is non-convex. In the following, we exploit the SCO technique to deal with this nonconvexity. Specifically, we need to find a concave lower bound to approximate the constraint function of (10b). From the fact that any convex function can be lower bounded by its first-order Taylor expansion at any point, we obtain the following concave lower bound at the local point $\alpha_{m,r}^{\{j\}}$

$$\begin{aligned}
&\widetilde{R}_1(\boldsymbol{\alpha})|_{\boldsymbol{\tau}^{\{j\}},\mathbf{P}^{\{j\}}} \\
&\geq \frac{\tau_m^{\{j\}}}{N}\Bigg[\log\left(C_{m,r}+\Big(\sum_{k=0}^{N-1} P_{m,k}^{\{j\}}\alpha_{m,r}A_{m,r,k}\Big)^2\right) \\
&\quad - \ldots \log\left(C_{m,r}^{\{j\}}\right) \\
&\quad - \ldots \frac{\sum_{k=0}^{N-1} P_{m,k}^{\{j\}}A_{m,r,k}(\alpha_{m,r}^{\{j\}}\sum_{i=r+1}^{R} P_{m,k}^{\{j\}}A_{m,i,k})\tilde{\alpha}_{m,r}^{\{j\}}}{C_{m,r}^{\{j\}}} \\
&\quad - \ldots \frac{\sum_{k=0}^{N-1} P_{m,k}^{\{j\}}A_{m,r,k}[(\sigma^2+\sum_{i=r+1}^{R} P_{m,k}^{\{j\}}\alpha_{m,i}^{\{j\}}A_{m,i,k})\tilde{\alpha}_{m,r}^{\{j\}}]}{C_{m,r}^{\{j\}}}\Bigg] \\
&\triangleq \widehat{R}_1^{\text{lb}}(\boldsymbol{\alpha})|_{\boldsymbol{\tau}^{\{j\}},\mathbf{P}^{\{j\}}}, \quad \forall m, 1 \leq r \leq R-1
\end{aligned} \tag{14}$$

where $\tilde{\alpha}_{m,r}^{\{j\}} = \alpha_{m,r} - \alpha_{m,r}^{\{j\}}$.

Similarly, we obtain the following lower bound on the constraint function of (10c)

$$\begin{aligned}
&\widetilde{R}_2(\boldsymbol{\alpha})|_{\boldsymbol{\tau}^{\{j\}},\mathbf{P}^{\{j\}}} \\
&\geq \sum_{m=1}^{M}\frac{\tau_m^{\{j\}}}{N}\sum_{k=0}^{N-1}\Bigg[\log\left(P_{m,k}^{\{j\}}\sum_{r=1}^{R}\alpha_{m,r}B_{m,r,k}+P_{m,k}^{\{j\}}|H_k|^2+\sigma^2\right) \\
&\quad - \log\left(P_{m,k}^{\{j\}}\sum_{r=1}^{R}\alpha_{m,r}^{\{j\}}B_{m,r,k}+\sigma^2\right) \\
&\quad - \frac{P_{m,k}^{\{j\}}\sum_{r=1}^{R}B_{m,r,k}(\alpha_{m,r}-\alpha_{m,r}^{\{j\}})}{P_{m,k}^{\{j\}}\sum_{i=1}^{R}\alpha_{m,r}^{\{j\}}B_{m,r,k}+\sigma^2}\Bigg] \\
&\triangleq \widehat{R}_2^{\text{lb}}(\boldsymbol{\alpha})|_{\boldsymbol{\tau}^{\{j\}},\mathbf{P}^{\{j\}}}.
\end{aligned} \tag{15}$$

With given local points $\boldsymbol{\alpha}^{\{j\}}$ and lower bounds $\widehat{R}_1^{\text{lb}}(\boldsymbol{\alpha})|_{\boldsymbol{\tau}^{\{j\}},\mathbf{P}^{\{j\}}}$ and $\widehat{R}_2^{\text{lb}}(\boldsymbol{\alpha})|_{\boldsymbol{\tau}^{\{j\}},\mathbf{P}^{\{j\}}}$, by introducing two slack variables $Q_{\text{rpa1}}^{\text{lb}}$ (“rpa” means “reflection power allocation”) and $D_{\text{rpa}}^{\text{lb}}$ for the BD-throughput constraints and LU-throughput constraint, respectively, problem (12) is approximated as

$$\text{(P1-b')}: \max_{Q_{\text{rpa1}}^{\text{lb}},D_{\text{rpa}}^{\text{lb}},\boldsymbol{\alpha}} \quad Q_{\text{rpa1}}^{\text{lb}} \tag{16a}$$

$$\text{s.t. } \widehat{R}_1^{\text{lb}}(\boldsymbol{\alpha})|_{\boldsymbol{\tau}^{\{j\}},\mathbf{P}^{\{j\}}} \geq Q_{\text{rpa1}}^{\text{lb}}, \quad \forall m,\ r = 1, 2 \ldots R-1 \tag{16b}$$

$$\frac{\tau_m^{\{j\}}}{N}\log\left(1+\sum_{k=0}^{N-1}\frac{P_{m,k}^{\{j\}}\alpha_{m,R}A_{m,R,k}}{\sigma^2}\right)\geq Q_{\mathsf{rpa1}}^{\mathsf{lb}},\quad \forall m \tag{16c}$$

$$\widehat{R}_2^{\mathsf{lb}}(\boldsymbol{\alpha})|_{\boldsymbol{\tau}^{\{j\}},\mathbf{P}^{\{j\}}}\geq D_{\mathsf{rpa}}^{\mathsf{lb}}, \tag{16d}$$

$$(10d),\ (10i). \tag{16e}$$

Problem (16) is a convex optimization problem which can also be efficiently solved by CVX. It is worth noting that the feasible set of problem (16) is always a subset of that of problem (12) for the lower bounds taken in (16b), (16c), and (16d). Therefore, the optimal objective value of problem (16) is a lower bound of that of problem (12).

3) SUBCARRIER POWER ALLOCATION OPTIMIZATION

For given backscatter time allocation vector $\boldsymbol{\tau}^{\{j\}}$ and power reflection coefficient vector $\boldsymbol{\alpha}^{\{j\}}$, the subcarrier power allocation matrix $\mathbf{P}$ can be optimized by solving

$$(\text{P1-c}):\ \max_{Q,\mathbf{P}}\quad Q \tag{17a}$$

$$\text{s.t. } (10b),\ (10c),\ (10d),\ (10e),\ (10h). \tag{17b}$$

Notice that the constraint function $\widetilde{R}_3(\mathbf{P})|_{\boldsymbol{\tau}^{\{j\}},\boldsymbol{\alpha}^{\{j\}}}$ in (10b) and $\widetilde{R}_4(\mathbf{P})|_{\boldsymbol{\tau}^{\{j\}},\boldsymbol{\alpha}^{\{j\}}}$ in (10c) are non-concave with respect to $P_{m,k}$, problem (17) is non-convex. After performing SCO method, we have the following concave lower bound at the local point $P_{m,k}^{\{j\}}$

$$\begin{aligned}&\widetilde{R}_3(\mathbf{P})|_{\boldsymbol{\tau}^{\{j\}},\boldsymbol{\alpha}^{\{j\}}}\\&\geq\frac{\tau_m^{\{j\}}}{N}\Bigg[\log\left(D_{m,r}+(\sum_{k=0}^{N-1}P_{m,k}\alpha_{m,r}^{\{j\}}A_{m,r,k})^2\right)\\&\quad-\ldots\log\left(D_{m,r}^{\{j\}}\right)-\frac{\sigma^2\sum_{k=0}^{N-1}\alpha_{m,r}^{\{j\}}A_{m,r,k}\widetilde{P}_{m,k}^{\{j\}}}{D_{m,r}^{\{j\}}}\\&\quad-\ldots\frac{2\sum_{k=0}^{N-1}P_{m,k}^{\{j\}}\alpha_{m,r}^{\{j\}}A_{m,r,k}\sum_{i=r+1}^{R}\alpha_{m,i}^{\{j\}}A_{m,i,k}\widetilde{P}_{m,k}^{\{j\}}}{D_{m,r}^{\{j\}}}\Bigg]\\&=\widehat{R}_3^{\mathsf{lb}}(\mathbf{P})|_{\boldsymbol{\tau}^{\{j\}},\boldsymbol{\alpha}^{\{j\}}},\quad \forall m,\ 1\leq r\leq R-1\end{aligned} \tag{18}$$

where we define $D_{m,r}=\sum_{k=0}^{N-1}[P_{m,k}\alpha_{m,r}^{\{j\}}A_{m,r,k}\times(\sum_{i=r+1}^{R}P_{m,k}\alpha_{m,i}^{\{j\}}A_{m,i,k}+\sigma^2)]$, $\widetilde{P}_{m,k}^{\{j\}}=P_{m,k}-P_{m,k}^{\{j\}}$, for convenience.

As such, we can obtain the following lower bound on the constraint function of (10c)

$$\begin{aligned}&\widetilde{R}_4(\mathbf{P})|_{\boldsymbol{\tau}^{\{j\}},\boldsymbol{\alpha}^{\{j\}}}\\&\geq\sum_{m=1}^{M}\frac{\tau_m^{\{j\}}}{N}\sum_{k=0}^{N-1}\Bigg[-\frac{\sum_{r=1}^{R}\alpha_{m,r}^{\{j\}}B_{m,r,k}(P_{m,k}-P_{m,k}^{\{j\}})}{P_{m,k}^{\{j\}}\sum_{i=1}^{R}\alpha_{m,r}^{\{j\}}B_{m,r,k}+\sigma^2}\\&\quad-\log\left(P_{m,k}^{\{j\}}\sum_{r=1}^{R}\alpha_{m,r}^{\{j\}}B_{m,r,k}+\sigma^2\right)\\&\quad+\log\left(P_{m,k}\sum_{r=1}^{R}\alpha_{m,r}^{\{j\}}B_{m,r,k}+P_{m,k}|H_k|^2+\sigma^2\right)\Bigg]\\&=\widehat{R}_4^{\mathsf{lb}}(\mathbf{P})|_{\boldsymbol{\tau}^{\{j\}},\boldsymbol{\alpha}^{\{j\}}}.\end{aligned} \tag{19}$$

With given local points $\mathbf{P}^{\{j\}}$ and lower bounds $\widehat{R}_3^{\mathsf{lb}}(\mathbf{P})|_{\boldsymbol{\tau}^{\{j\}},\boldsymbol{\alpha}^{\{j\}}}$ and $\widehat{R}_4^{\mathsf{lb}}(\mathbf{P})|_{\boldsymbol{\tau}^{\{j\}},\boldsymbol{\alpha}^{\{j\}}}$, by introducing two slack variables $Q_{\mathsf{spa}}^{\mathsf{lb1}}$("spa" means "subcarrier power allocation") and $D_{\mathsf{spa}}^{\mathsf{lb}}$ for the BD-throughput constraints and LU-throughput constraint, respectively, problem (17) is approximated as

$$(\text{P1-c'}):$$

$$\max_{Q_{\mathsf{spa1}}^{\mathsf{lb}},D_{\mathsf{spa}}^{\mathsf{lb}},\mathbf{P}}\quad Q_{\mathsf{spa1}}^{\mathsf{lb}} \tag{20a}$$

$$\text{s.t. } \widehat{R}_3^{\mathsf{lb}}(\mathbf{P})|_{\boldsymbol{\tau}^{\{j\}},\boldsymbol{\alpha}^{\{j\}}}\geq Q_{\mathsf{spa1}}^{\mathsf{lb}},\quad \forall m,\ r=1,2\ldots R-1 \tag{20b}$$

$$\frac{\tau_m^{\{j\}}}{N}\log\left(1+\sum_{k=0}^{N-1}\frac{P_{m,k}\alpha_{m,R}^{\{j\}}A_{m,R,k}}{\sigma^2}\right)\geq Q_{\mathsf{spa1}}^{\mathsf{lb}},\quad \forall m \tag{20c}$$

$$\widehat{R}_4^{\mathsf{lb}}(\mathbf{P})|_{\boldsymbol{\tau}^{\{j\}},\boldsymbol{\alpha}^{\{j\}}}\geq D_{\mathsf{spa}}^{\mathsf{lb}}, \tag{20d}$$

$$(10d),\ (10e),\ (10h). \tag{20e}$$

Similarly, problem (20) is a convex optimization problem that can be solved by CVX, and the optimal objective value obtained from problem (20) is in general a lower bound of that of problem (17).

B. SOLUTION FOR FSRN WITH EGC-BASED FAP

In this subsection, the case $i=2$ in (10b) is considered, which means that the FAP detects the BD signals based on EGC. Notice that the only difference between the formulated problems in the case of EGC and MRC is that the constraint function in (10b). The same parts of the discussion are omitted here for brevity.

1) BACKSCATTER TIME ALLOCATION OPTIMIZATION

In iteration $j, j\geq 1$, for given power reflection coefficient vector $\boldsymbol{\alpha}^{\{j\}}$ and subcarrier power allocation matrix $\mathbf{P}^{\{j\}}$, the backscatter time allocation vector $\boldsymbol{\tau}$ can be optimized by solving the following problem

$$(\text{P2-a}):\ \max_{Q,\boldsymbol{\tau}}\quad Q \tag{21a}$$

$$\text{s.t. } (10b),\ (10c),\ (10d),\ (10e),\ (10f),\ (10g). \tag{21b}$$

Problem (21) is also a standard LP and can be solved efficiently by CVX.

2) REFLECTION POWER ALLOCATION OPTIMIZATION

For given backscatter time allocation vector $\boldsymbol{\tau}^{\{j\}}$ and subcarrier power allocation matrix $\mathbf{P}^{\{j\}}$, the power reflection coefficient vector $\boldsymbol{\alpha}$ can be optimized by solving

$$(\text{P2-b}):\ \max_{Q,\boldsymbol{\alpha}}\quad Q \tag{22a}$$

$$\text{s.t. } (10b),\ (10c),\ (10d),\ (10i). \tag{22b}$$

Note that the constraint functions $\widetilde{R}_5(\boldsymbol{\alpha})|_{\boldsymbol{\tau}^{\{j\}},\mathbf{P}^{\{j\}}}$ in (10b) and $\widetilde{R}_2(\boldsymbol{\alpha})|_{\boldsymbol{\tau}^{\{j\}},\mathbf{P}^{\{j\}}}$ in (10c) are non-concave with respect to $\alpha_{m,r}$'s, problem (22) is non-convex. After exploiting SCO technique, we obtain the following lower bound on the constraint function $\widetilde{R}_5(\boldsymbol{\alpha})|_{\boldsymbol{\tau}^{\{j\}},\mathbf{P}^{\{j\}}}$ at the local point $\alpha_{m,r}^{\{j\}}$

$$\begin{aligned}
&\widetilde{R}_5(\boldsymbol{\alpha})|_{\boldsymbol{\tau}^{\{j\}},\mathbf{P}^{\{j\}}} \\
&\geq \frac{\tau_m^{\{j\}}}{N}\Bigg[\log\left(\sum_{k=0}^{N-1}P_{m,k}^{\{j\}}\sum_{i=r}^{R}\alpha_{m,i}A_{m,i,k}+N\sigma^2\right) \\
&\quad-\log\left(\sum_{k=0}^{N-1}\sum_{i=r+1}^{R}P_{m,k}^{\{j\}}\alpha_{m,i}^{\{j\}}A_{m,i,k}+N\sigma^2\right) \\
&\quad-\frac{\sum_{k=0}^{N-1}\sum_{i=r+1}^{R}P_{m,k}^{\{j\}}A_{m,i,k}(\alpha_{m,i}-\alpha_{m,i}^{\{j\}})}{\sum_{k=0}^{N-1}\sum_{i=r+1}^{R}P_{m,k}^{\{j\}}\alpha_{m,i}^{\{j\}}A_{m,i,k}+N\sigma^2}\Bigg] \\
&=\widehat{R}_5^{\mathsf{lb}}(\boldsymbol{\alpha})|_{\boldsymbol{\tau}^{\{j\}},\mathbf{P}^{\{j\}}},\quad \forall m,\,1\leq r\leq R-1. \qquad (23)
\end{aligned}$$

With given local points $\boldsymbol{\alpha}^{\{j\}}$ and lower bounds $\widehat{R}_5^{\mathsf{lb}}(\boldsymbol{\alpha})|_{\boldsymbol{\tau}^{\{j\}},\mathbf{P}^{\{j\}}}$ and $\widehat{R}_2^{\mathsf{lb}}(\boldsymbol{\alpha})|_{\boldsymbol{\tau}^{\{j\}},\mathbf{P}^{\{j\}}}$, by introducing two slack variables $Q_{\mathsf{rpa2}}^{\mathsf{lb}}$ and $D_{\mathsf{rpa}}^{\mathsf{lb}}$ for the BD-throughput constraints and LU-throughput constraint, respectively, problem (22) is approximated as

(P2-b') :

$$\max_{Q_{\mathsf{rpa2}}^{\mathsf{lb}},D_{\mathsf{rpa}}^{\mathsf{lb}},\boldsymbol{\alpha}} \quad Q_{\mathsf{rpa2}}^{\mathsf{lb}} \qquad (24a)$$

$$\text{s.t. } \widehat{R}_5^{\mathsf{lb}}(\boldsymbol{\alpha})|_{\boldsymbol{\tau}^{\{j\}},\mathbf{P}^{\{j\}}}\geq Q_{\mathsf{rpa2}}^{\mathsf{lb}},\quad \forall m,\ r=1,2\ldots R-1 \qquad (24b)$$

$$\frac{\tau_m^{\{j\}}}{N}\log\left(1+\sum_{k=0}^{N-1}\frac{P_{m,k}^{\{j\}}\alpha_{m,R}A_{m,R,k}}{N\sigma^2}\right)\geq Q_{\mathsf{rpa2}}^{\mathsf{lb}},\quad \forall m \qquad (24c)$$

$$\widehat{R}_2^{\mathsf{lb}}(\boldsymbol{\alpha})|_{\boldsymbol{\tau}^{\{j\}},\mathbf{P}^{\{j\}}}\geq D_{\mathsf{rpa}}^{\mathsf{lb}}, \qquad (24d)$$

$$(10d),\ (10i). \qquad (24e)$$

Problem (24) is a convex optimization problem which can be solved by CVX, and the optimal objective value obtained from problem (24) is in general a lower bound of that of problem (22).

3) SUBCARRIER POWER ALLOCATION OPTIMIZATION

For given backscatter time allocation vector $\boldsymbol{\tau}^{\{j\}}$ and power reflection coefficient vector $\boldsymbol{\alpha}^{\{j\}}$, the subcarrier power allocation matrix $\mathbf{P}$ can be optimized by solving

$$(\text{P2-c}):\ \max_{Q,\mathbf{P}}\quad Q \qquad (25a)$$

$$\text{s.t. } (10b),\ (10c),\ (10d),\ (10e),\ (10h). \qquad (25b)$$

Notice that the constraint functions $\widetilde{R}_6(\mathbf{P})|_{\boldsymbol{\tau}^{\{j\}},\boldsymbol{\alpha}^{\{j\}}}$ in (10b) and $\widetilde{R}_4(\mathbf{P})|_{\boldsymbol{\tau}^{\{j\}},\boldsymbol{\alpha}^{\{j\}}}$ in (10c) are non-concave with respect to $P_{m,k}$, problem (25) is non-convex. After performing SCO method, we obtain the following lower bound on the constraint function $\widetilde{R}_6(\boldsymbol{\alpha})|_{\boldsymbol{\tau}^{\{j\}},\mathbf{P}^{\{j\}}}$ at the local point $P_{m,k}^{\{j\}}$

$$\begin{aligned}
&\widetilde{R}_6(\mathbf{P})|_{\boldsymbol{\tau}^{\{j\}},\boldsymbol{\alpha}^{\{j\}}} \\
&\geq \frac{\tau_m^{\{j\}}}{N}\Bigg[\log\left(\sum_{k=0}^{N-1}P_{m,k}\sum_{i=r}^{R}\alpha_{m,i}^{\{j\}}A_{m,i,k}+N\sigma^2\right) \\
&\quad-\log\left(\sum_{k=0}^{N-1}\sum_{i=r+1}^{R}P_{m,k}^{\{j\}}\alpha_{m,i}^{\{j\}}A_{m,i,k}+N\sigma^2\right) \\
&\quad-\frac{\sum_{k=0}^{N-1}\sum_{i=r+1}^{R}\alpha_{m,i}^{\{j\}}A_{m,i,k}(P_{m,k}-P_{m,k}^{\{j\}})}{\sum_{k=0}^{N-1}\sum_{i=r+1}^{R}P_{m,k}^{\{j\}}\alpha_{m,i}^{\{j\}}A_{m,i,k}+N\sigma^2}\Bigg] \\
&=\widehat{R}_6^{\mathsf{lb}}(\mathbf{P})|_{\boldsymbol{\tau}^{\{j\}},\boldsymbol{\alpha}^{\{j\}}},\quad \forall m,\,1\leq r\leq R-1. \qquad (26)
\end{aligned}$$

With given local points $\mathbf{P}^{\{j\}}$ and lower bounds $\widehat{R}_6^{\mathsf{lb}}(\mathbf{P})|_{\boldsymbol{\tau}^{\{j\}},\boldsymbol{\alpha}^{\{j\}}}$ and $\widehat{R}_4^{\mathsf{lb}}(\mathbf{P})|_{\boldsymbol{\tau}^{\{j\}},\boldsymbol{\alpha}^{\{j\}}}$, by introducing two slack variables $Q_{\mathsf{spa2}}^{\mathsf{lb}}$ and $D_{\mathsf{spa}}^{\mathsf{lb}}$ for the BD-throughput constraints and LU-throughput constraint, respectively, problem (25) is approximated as

(P2-c') :

$$\max_{Q_{\mathsf{spa2}}^{\mathsf{lb}},D_{\mathsf{spa}}^{\mathsf{lb}},\mathbf{P}} \quad Q_{\mathsf{spa2}}^{\mathsf{lb}} \qquad (27a)$$

$$\text{s.t. } \widehat{R}_6^{\mathsf{lb}}(\mathbf{P})|_{\boldsymbol{\tau}^{\{j\}},\boldsymbol{\alpha}^{\{j\}}}\geq Q_{\mathsf{spa2}}^{\mathsf{lb}},\quad \forall m,\ r=1,2\ldots R-1 \qquad (27b)$$

$$\frac{\tau_m^{\{j\}}}{N}\log\left(1+\sum_{k=0}^{N-1}\frac{P_{m,k}\alpha_{m,R}^{\{j\}}A_{m,R,k}}{N\sigma^2}\right)\geq Q_{\mathsf{spa2}}^{\mathsf{lb}},\quad \forall m \qquad (27c)$$

$$\widehat{R}_4^{\mathsf{lb}}(\mathbf{P})|_{\boldsymbol{\tau}^{\{j\}},\boldsymbol{\alpha}^{\{j\}}}\geq D_{\mathsf{spa}}^{\mathsf{lb}}, \qquad (27d)$$

$$(10d),\ (10e),\ (10h). \qquad (27e)$$

Similarly, problem (27) is a convex optimization problem that can be solved by CVX, and the optimal objective value obtained from problem (27) is in general a lower bound of that of problem (25).

C. OVERALL ALGORITHM

When the FAP detects the BD signals based on either MRC or EGC, there are three blocks of variables to be optimized, i.e., $\mathbf{P}$, $\boldsymbol{\tau}$, and $\boldsymbol{\alpha}$. We use the BCD technique to obtain the optimal (suboptimal) solution iteratively. In each iteration, we optimize one block of variables with the other two blocks of variables fixed, and the optimal (suboptimal) solution of the variable obtained in this iteration is served as the input of the next iteration. The details are summarized in Algorithm 1.

The convergence of BCD algorithm requires that each subproblem should be solved optimally while optimizing one block of variables in each iteration [37]. In the above algorithm 1, we only solve the approximate subproblems of the original subproblems (P1-b), (P1-c), (P2-b), and (P2-c),

Algorithm 1 Proposed Iterative Algorithm for Solving Problem (P1) or (P2)

1: Initialize $\mathbf{P}^{\{0\}}, \boldsymbol{\tau}^{\{0\}}, \boldsymbol{\alpha}^{\{0\}}, Q^{\{0\}}$ with $P_{m,k}^{\{0\}} = \frac{1}{MN}$, $\tau_m^{\{0\}} = \frac{1}{M}$, $\alpha_{(m,r)}^{\{0\}} = 0.5$, $Q^{\{0\}} = 100$, and set small threshold constant $\epsilon = 10^{-4}$. Let $j = 0$.
2: **while** $|Q^{\{j+1\}} - Q^{\{j\}}| \geq \epsilon$ **do**
3: Solve (P1-a) or (P2-a) under fixed $\boldsymbol{\alpha}^{\{j\}}$ and $\mathbf{P}^{\{j\}}$, and the optimal solution is obtained as $\boldsymbol{\tau}^{\{j+1\}}$.
4: Solve (P1-b') or (P2-b') under fixed $\boldsymbol{\tau}^{\{j+1\}}$, $\mathbf{P}^{\{j\}}$, and $\boldsymbol{\alpha}^{\{j\}}$, and the optimal solution is obtained as $\boldsymbol{\alpha}^{\{j+1\}}$.
5: Solve (P1-c') or (P2-c') under fixed $\boldsymbol{\tau}^{\{j+1\}}$, $\boldsymbol{\alpha}^{\{j+1\}}$, and $\mathbf{P}^{\{j\}}$, and the optimal solution is obtained as $\mathbf{P}^{\{j+1\}}$.
6: Update iteration index $j = j + 1$.
7: **end while**
8: Return the optimal solution $\mathbf{P}^{\star} = \mathbf{P}^{\{j-1\}}$, $\boldsymbol{\tau}^{\star} = \boldsymbol{\tau}^{\{j-1\}}$ and $\boldsymbol{\alpha}^{\star} = \boldsymbol{\alpha}^{\{j-1\}}$.

thus the convergence of Algorithm 1 needs to be verified, as follows.

Theorem 1: Algorithm 1 is guaranteed to converge.

Proof: In step 3, we obtain the optimal solution $\boldsymbol{\tau}^{\{j+1\}}$ under fixed $\boldsymbol{\alpha}^{\{j\}}$ and $\mathbf{P}^{\{j\}}$, thus the minimum throughput satisfies the following inequality

$$Q(\boldsymbol{\tau}^{\{j\}}, \boldsymbol{\alpha}^{\{j\}}, \mathbf{P}^{\{j\}}) \leq Q(\boldsymbol{\tau}^{\{j+1\}}, \boldsymbol{\alpha}^{\{j\}}, \mathbf{P}^{\{j\}}). \tag{28}$$

In step 4, we obtain the suboptimal solution $\boldsymbol{\alpha}^{\{j+1\}}$ based on SCO method, under fixed $\boldsymbol{\tau}^{\{j+1\}}$ and $\mathbf{P}^{\{j\}}$. The following relationships are established

$$\begin{aligned} Q(\boldsymbol{\tau}^{\{j+1\}}, \boldsymbol{\alpha}^{\{j\}}, \mathbf{P}^{\{j\}}) &\overset{(a1)}{=} Q_{\mathsf{rpa}}^{\mathsf{lb}}(\boldsymbol{\tau}^{\{j+1\}}, \boldsymbol{\alpha}^{\{j\}}, \mathbf{P}^{\{j\}}) \\ &\overset{(b1)}{\leq} Q_{\mathsf{rpa}}^{\mathsf{lb}}(\boldsymbol{\tau}^{\{j+1\}}, \boldsymbol{\alpha}^{\{j+1\}}, \mathbf{P}^{\{j\}}) \\ &\overset{(c1)}{\leq} Q(\boldsymbol{\tau}^{\{j+1\}}, \boldsymbol{\alpha}^{\{j+1\}}, \mathbf{P}^{\{j\}}), \end{aligned} \tag{29}$$

where (a1) comes from that the Taylor expansions in (14), (15), and (23) are tight at given local points, which indicates that the objective functions of (P1-b) and (P2-b) at $\boldsymbol{\alpha}^{\{j\}}$ are the same as that of (P1-b') and (P2-b'), respectively; (b1) is true since the optimal solutions to (P1-b') and (P2-b') are $\boldsymbol{\alpha}^{\{j+1\}}$; (c1) is because the objective values of original problems (P1-b) and (P2-b) are lower bounded by that of problem (P1-b') and (P2-b'), respectively.

Similarly, in step 5, the minimum throughput satisfies the following relationships

$$\begin{aligned} Q(\boldsymbol{\tau}^{\{j+1\}}, \boldsymbol{\alpha}^{\{j+1\}}, \mathbf{P}^{\{j\}}) &\overset{(a2)}{=} Q_{\mathsf{spa}}^{\mathsf{lb}}(\boldsymbol{\tau}^{\{j+1\}}, \boldsymbol{\alpha}^{\{j+1\}}, \mathbf{P}^{\{j\}}) \\ &\overset{(b2)}{\leq} Q_{\mathsf{spa}}^{\mathsf{lb}}(\boldsymbol{\tau}^{\{j+1\}}, \boldsymbol{\alpha}^{\{j+1\}}, \mathbf{P}^{\{j+1\}}) \\ &\overset{(c2)}{\leq} Q(\boldsymbol{\tau}^{\{j+1\}}, \boldsymbol{\alpha}^{\{j+1\}}, \mathbf{P}^{\{j+1\}}), \end{aligned} \tag{30}$$

as such, (a2) comes from that the Taylor expansions in (18), (19), and (26) are tight at given local points, which indicates that the objective functions of (P1-c) and (P2-c) at $P^{\{j\}}$ are the same as that of (P1-c') and (P2-c'), respectively; (b2) is true since the optimal solutions to (P1-c') and (P2-c') are $P^{\{j+1\}}$; (c2) is because the objective values of original problems (P1-c) and (P2-c) are lower bounded by that of problem (P1-c') and (P2-c'), respectively.

From (28), (29), and (30), it is straightforward that

$$Q(\boldsymbol{\tau}^{\{j\}}, \boldsymbol{\alpha}^{\{j\}}, \mathbf{P}^{\{j\}}) \leq Q(\boldsymbol{\tau}^{\{j+1\}}, \boldsymbol{\alpha}^{\{j+1\}}, \mathbf{P}^{\{j+1\}}). \tag{31}$$

The inequality (31) indicates that the objective values of (P1) and (P2) are always non-decreasing after each iteration. Besides, the objective values of (P1) and (P2) are upper-bounded by some finite positive number, since the objective function is continues over the compact feasible set. Therefore, the proposed Algorithm 1 is guaranteed to converge. The convergence proof is completed. □

It is noted that Algorithm 1 can obtain a (locally at least) optimal solution, although multiple first-order Taylor approximations are used. As shown in the above proof steps, a better objective value can be obtained after each iteration, the variables will get closer and closer to the optimal points, as the number of iterations increases. The first-order Taylor expansion is getting tighter as the algorithm converges, which is also adopted and shown in references like [40].

Since only three convex optimization problems need to be solved in each iteration, the algorithm's complexity is affordable. Moreover, as will be numerically shown in Section V, Algorithm 1 converges in about five iterations. Therefore, the proposed Algorithm 1 can be practically implemented with fast convergence for an FSRN.

V. NUMERICAL RESULTS

This section provides numerical results. We consider independent Rayleigh fading channels and the power gains of multiple paths are exponentially distributed. For each channel link, its first-path channel power gain is assumed to be $10^{-3}d^{-2.5}$, where d is the distance with unit of meter (m). We assume the number of multi-path channels to be $L_{\mathsf{f}} = L_{\mathsf{g}} = 4$, $L_{\mathsf{h}} = 8$, and $L_{\mathsf{v}} = 6$. We fix $M = 2, R = 2$, i.e., four BDs are considered. The OFDM parameters are $N = 64, N_{\mathsf{cp}} = 16$. Let $\bar{E}_{m,r} = E_{\min}, \forall m, r$. We set $\bar{P} = 1, \epsilon = 10^{-4}$, and $\eta_{m,r} = 0.5$. The FAP-to-LU distance is 7 m. The FAP-to-BD distances are 3.8 m, 3.6 m, 2.2 m, and 2 m for BD 1, 2, 3, and 4, respectively. The BD-to-LU distances are 5 m, 6 m, 7 m, 8 m for BD 1, 2, 3, and 4, respectively. The BDs adopt the instantaneous-channel-power-based dynamic head-tail paring strategy which was given in Theorem 4 and proved to be optimal for max-min rate optimization in uplink NOMA [22]. The results are based on 1000 channel realizations. For comparison, we consider a benchmark scheme of dynamic TDMA, in which the four BDs individually backscatter signals to the FAP in four orthogonal slots and the slot durations are optimized to maximize the minimum throughput among all BDs. Notice that as in [37], the exhaustive approach is not considered as a benchmark in this section, since its complexity for the problem (10) with four blocks of continuous-value variables is too high. Parameter settings are summarized in Table 1.

TABLE 1. Parameter settings.

First-path channel power gain	$10^{-3}d^{-2.5}$
Number of multi-path of fading channels	$L_{\mathsf{f}} = L_{\mathsf{g}} = 4$, $L_{\mathsf{h}} = 8$, $L_{\mathsf{v}} = 6$
FAP-to-LU distance	7 m
FAP-to-BD 1 distance	3.8 m
FAP-to-BD 2 distance	3.6 m
FAP-to-BD 3 distance	2.2 m
FAP-to-BD 4 distance	2 m
BD 1-to-LU distance	5 m
BD 2-to-LU distance	6 m
BD 3-to-LU distance	7 m
BD 4-to-LU distance	8 m
Number of transmission slots	$M = 2$
Number of energy groups	$R = 2$
Number of subcarriers	$N = 64$
Length of cyclic prefix	$N_{cp} = 16$
Required minimum energy	$\bar{E}_{m,r} = 1.38 \times 10^{-7} J$
Maximum transmission power	$\bar{P} = 1$
Peak-power of each subcarrier	$P_{\text{peak}} = 20\frac{\bar{P}}{MN}$
Threshold ϵ of Algorithm 1	$\epsilon = 10^{-4}$
Energy-harvesting efficiency constant	$\eta_{m,r} = 0.5$
Channel realizations	1000

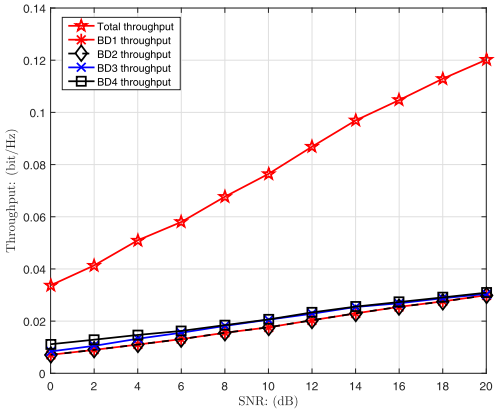

FIGURE 2. BDs' throughput versus SNR (NOMA-DTDMA, MRC).

Fig. 2 and Fig. 3 plot the BDs' throughput versus SNR for the proposed NOMA-DTDMA scheme in the case that the FAP performs MRC and EGC, respectively. Both Fig. 2 and Fig. 3 show that BDs' total throughput increases as SNR increases. From Fig. 2 and Fig. 3, moreover, we observe that BD 1 and BD 2 with weaker (average) channel strength, achieve almost the same throughput, which is comparable to those of BD 3 and BD 4 with stronger channel strength. This verifies that throughput fairness among all BDs can

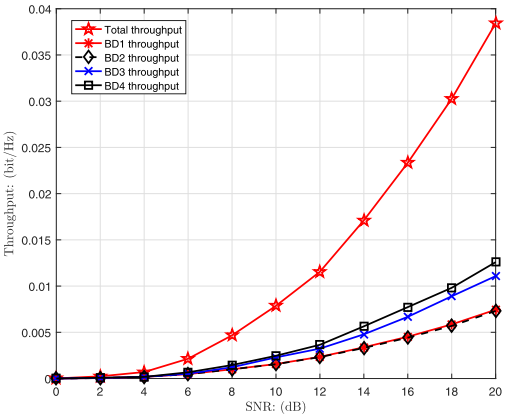

FIGURE 3. BDs' throughput versus SNR (NOMA-DTDMA, EGC).

be achieved by the proposed NOMA-DTDMA scheme. Furthermore, notice that the gap of BDs' throughput in Fig. 2 is smaller than that in Fig. 3, which implies that MRC outperforms EGC in terms of BD fairness for the proposed NOMA-DTDMA scheme.

Fig. 4 compares the BDs' total throughput for the proposed NOMA-DTDMA scheme and the benchmark of the dynamic TDMA scheme. We observe that the proposed scheme achieves significant throughput gain compared to the benchmark scheme. For instance, in the case that the FAP detects BDs' signals based on MRC, the total throughput of the NOMA-DTDMA scheme is 195.61%, 117.70% and 98.63% higher than that of the dynamic TDMA scheme when the SNR is 0, 10 and 20 dB, respectively. In addition, MRC achieves higher throughput than EGC with the same SNR for the proposed NOMA-DTDMA scheme, and the gap between them is enlarged as SNR increases. The reason is that the selection of weighting gains in MRC can strengthen the effect of high SNR branch and weaken the effect of low SNR branch, while all the branches have the same weighting gain in EGC. However, when the FAP-BD-FAP product channel coefficients (MRC's weighting coefficients) are

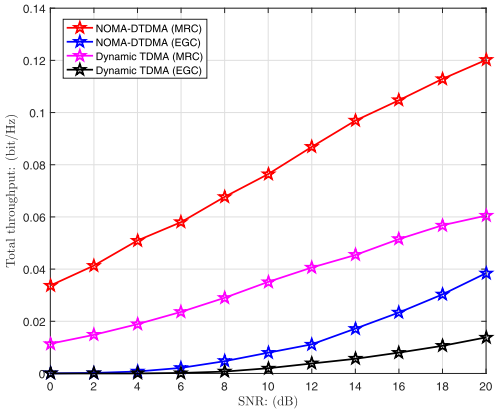

FIGURE 4. Comparison of BDs' total throughput between NOMA-DTDMA and dynamic TDMA versus SNR.

unknown or it is advisable to apply EGC which needs only the phase information of the channel coefficients. There is a tradeoff between performance and complexity.

Fig. 5 plots the BDs' total throughput versus the LU's throughput requirement D under different SNRs (i.e., 0 and 10 dB). As expected, the BDs' total throughput with SNR = 10 dB is far greater than that with SNR = 0 dB at same D both for the proposed NOMA-DTDMA scheme and the dynamic TDMA scheme. We further observe that the BDs' total throughput decreases as the LU's throughput requirement D increases, indicating the trade-off performance between the BDs and LU in terms of throughput. Moreover, considering SNR = 10 dB,the BDs' total throughput for the proposed NOMA-DTDMA scheme based on MRC is 98.71%, 104.94%, and 288.52% higher than that of dynamic TDMA scheme based on MRC when D is 1, 3, and 5 bps/Hz, respectively.

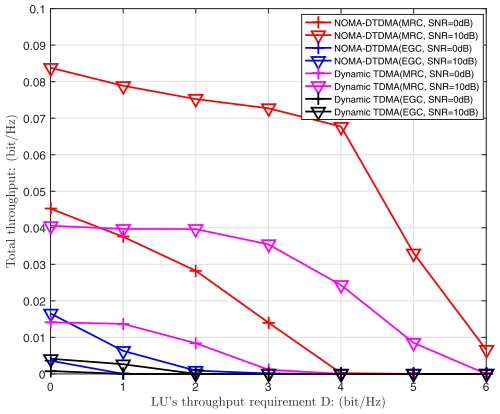

FIGURE 5. BDs' total throughput versus LU's throughput requirement D under different SNRs.

Fig. 6 plots the BDs' total throughput versus the BDs' harvested energy requirement $E_{\min}$ under different SNRs (i.e., 0 and 10 dB). Similarly, the BDs' total throughput with SNR = 10 dB is significantly greater than that with SNR = 0 dB at the same $E_{\min}$ for both the proposed NOMA-DTDMA scheme and the benchmark dynamic TDMA scheme. Also, we observe that the BDs' total throughput decreases as $E_{\min}$ increases, indicating the tradeoff performance between the BDs' throughput and harvested energy requirement. Furthermore, it is shown that when $E_{\min}$ is greater than 23 millijoules, even the proposed NOMA-DTDMA scheme based on MRC with SNR = 0 dB achieves higher throughput than the dynamic TDMA scheme based on MRC with SNR = 10 dB.

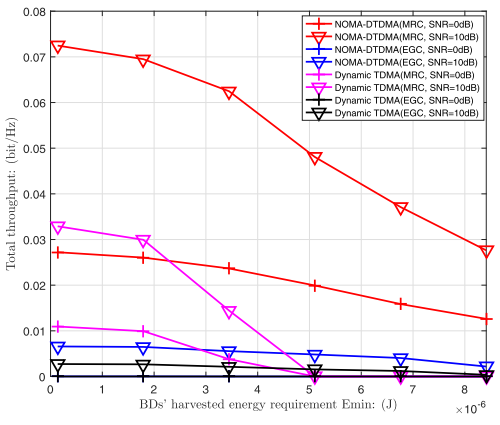

FIGURE 6. BDs' total throughput versus BDs' harvested energy requirement E under different SNRs.

Fig. 7 plots the BDs' total throughput versus the number of subcarriers N at SNR = 10 dB. It's shown that the BDs' total throughput decreases as N increases. The reason is that the power allocated to each subcarrier decreases in general as N increases, since the FAP's maximum transmission-power $\bar{P}$ is a constant value. The throughput gain obtained by the combining technique cannot compensate for the reduction of subcarrier power.

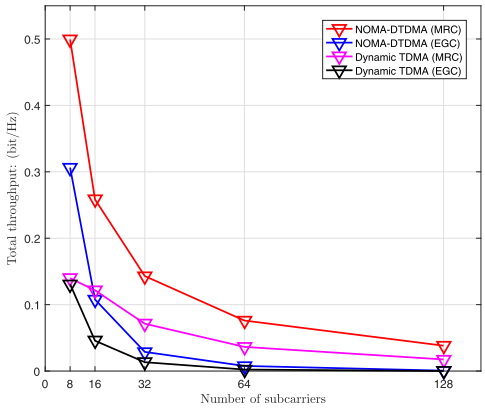

FIGURE 7. BDs' total throughput versus the number of subcarriers N under different SNRs.

Fig. 8 plots the average convergence performance of the proposed Algorithm 1. We observe that the NOMA-DTDMA scheme based on either MRC or EGC takes about five iterations to converge. The converged average max-min throughput is 0.0156 bit/Hz and 0.00170 bit/Hz for MRC and EGC, respectively. Thus, the convergence speed of Algorithm 1 is fast.

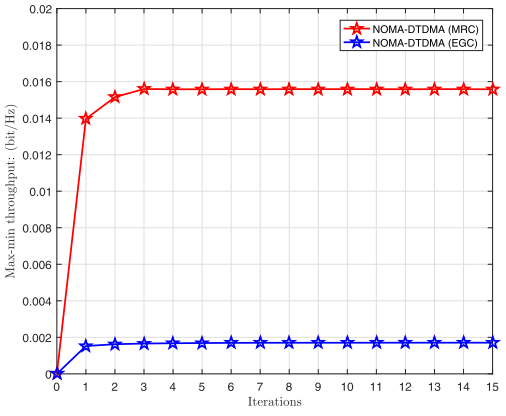

FIGURE 8. Convergence behavior of Algorithm 1.

In order to evaluate the effect of distance on the throughput performance, we scale the distances between all pairs of nodes by a positive factor $\theta > 0$. Fig. 9 plots the BDs' total throughput versus the distance scaling factor θ, for different LU's throughput requirements D's. It is observed that the BDs' total throughput decreases as θ increases, since the increase of distance weakens the channel strength. It is reasonable to choose the previous distance values with $\theta = 1$, which is practical for smart-home applications. In addition, the tradeoff between the BDs' total throughput and the LU's throughput is observed in Fig. 9.

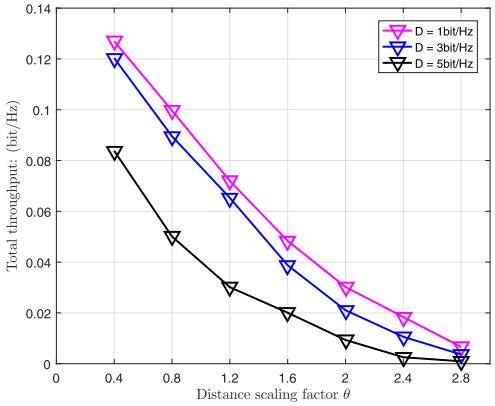

FIGURE 9. BDs' total throughput versus the distance scaling factor θ (NOMA-DTDMA, MRC).

VI. CONCLUSION

This paper has studied the resource allocation problem in a NOMA-enhanced FSRN. A NOMA-DTDMA transmission scheme is proposed to exploit the channel dynamics and further improve the spectrum efficiency. The minimum throughput among all BDs is maximized by jointly optimizing the FAP's subcarrier power allocation, the BDs' backscatter time and power reflection coefficients, subject to the LU's throughput requirement, the BDs' harvested energy requirements, and other practical constraints. An efficient iterative algorithm based on block coordinated descent and successive convex optimization techniques is proposed to obtain a suboptimal solution to the formulated non-convex problem. Numerical results show that the proposed NOMA-DTDMA scheme significantly outperforms the benchmark dynamic-TDMA scheme in terms of both throughput performance and BD fairness. Moreover, the tradeoff performances between the BDs' throughput and the LU's throughput requirement as well as the BDs' harvested energy requirements are numerically verified. This work can be further extended to the scenarios like a multi-antenna FAP and imperfect channel state information in practice.

REFERENCES

[1] J. A. Stankovic, "Research directions for the Internet of Things," *IEEE Internet Things J.*, vol. 1, no. 1, pp. 3–9, Feb. 2014.
[2] L. Atzori, A. Iera, and G. Morabito, "The Internet of Things: A survey," *Comput. Netw.*, vol. 54, no. 15, pp. 2787–2805, Oct. 2010.
[3] J. Lin, W. Yu, N. Zhang, X. Yang, H. Zhang, and W. Zhao, "A survey on Internet of Things: Architecture, enabling technologies, security and privacy, and applications," *IEEE Internet Things J.*, vol. 4, no. 5, pp. 1125–1142, Oct. 2017.
[4] L. Zhang, Y.-C. Liang, and M. Xiao, "Spectrum sharing for Internet of Things: A survey," *IEEE Wireless Commun.*, vol. 26, no. 3, pp. 132–139, Jun. 2019.
[5] G. Yang, C. K. Ho, and Y. L. Guan, "Multi-antenna wireless energy transfer for backscatter communication systems," *IEEE J. Select. Areas Commun.*, vol. 33, no. 12, pp. 2974–2987, Dec. 2015.
[6] A. Bletsas, P. N. Alevizos, and G. Vougioukas, "The art of signal processing in backscatter radio for μw (or less) Internet of Things: Intelligent signal processing and backscatter radio enabling batteryless connectivity," *IEEE Signal Process. Mag.*, vol. 35, no. 5, pp. 28–40, Sep. 2018.
[7] G. Yang, Y.-C. Liang, R. Zhang, and Y. Pei, "Modulation in the air: Backscatter communication over ambient OFDM carrier," *IEEE Trans. Commun.*, vol. 66, no. 3, pp. 1219–1233, Mar. 2018.
[8] Q. Zhang, H. Guo, Y.-C. Liang, and X. Yuan, "Constellation learning-based signal detection for ambient backscatter communication systems," *IEEE J. Sel. Areas Commun.*, vol. 37, no. 2, pp. 452–463, Feb. 2019.
[9] G. Yang, R. Dai, and Y.-C. Liang, "Energy-efficient UAV backscatter communication with joint trajectory design and resource optimization," 2019, *arXiv:1911.05553*. [Online]. Available: https://arxiv.org/abs/1911.05553
[10] G. Yang, Q. Zhang, and Y.-C. Liang, "Cooperative ambient backscatter communications for green Internet-of-Things," *IEEE Internet Things J.*, vol. 5, no. 2, pp. 1116–1130, Apr. 2018.
[11] R. Long, Y.-C. Liang, H. Guo, G. Yang, and R. Zhang, "Symbiotic radio: A new communication paradigm for passive Internet-of-Things," *IEEE Internet Things J.*, to be published, doi: 10.1109/jiot.2019.2954678.
[12] Y.-C. Liang, R. Long, Q. Zhang, J. Chen, H. V. Cheng, and H. Guo, "Large intelligent surface/antennas (LISA): Making reflective radios smart," *J. Commun. Inf. Netw.*, vol. 4, no. 2, pp. 40–50, Jun. 2019.
[13] D. Darsena, G. Gelli, and F. Verde, "Modeling and performance analysis of wireless networks with ambient backscatter devices," *IEEE Trans. Commun.*, vol. 65, no. 4, pp. 1797–1814, Apr. 2017.
[14] R. Long, H. Guo, L. Zhang, and Y.-C. Liang, "Full-duplex backscatter communications in symbiotic radio systems," *IEEE Access*, vol. 7, pp. 21597–21608, 2019.
[15] Q. Zhang, L. Zhang, Y.-C. Liang, and P.-Y. Kam, "Backscatter-NOMA: A symbiotic system of cellular and Internet-of-Things networks," *IEEE Access*, vol. 7, pp. 20000–20013, 2019.
[16] Z. Ding, X. Lei, G. K. Karagiannidis, R. Schober, J. Yuan, and V. K. Bhargava, "A survey on non-orthogonal multiple access for 5G networks: Research challenges and future trends," *IEEE J. Sel. Areas Commun.*, vol. 35, no. 10, pp. 2181–2195, Oct. 2017.
[17] L. Dai, B. Wang, Z. Ding, Z. Wang, S. Chen, and L. Hanzo, "A survey of non-orthogonal multiple access for 5G," *IEEE Commun. Surveys Tuts.*, vol. 20, no. 3, pp. 2294–2323, 3rd Quart., 2018.
[18] W. Shin, M. Vaezi, B. Lee, D. J. Love, J. Lee, and H. V. Poor, "Non-orthogonal multiple access in multi-cell networks: Theory, performance, and practical challenges," *IEEE Commun. Mag.*, vol. 55, no. 10, pp. 176–183, Oct. 2017.
[19] S. M. R. Islam, N. Avazov, O. A. Dobre, and K. Kwak, "Power-domain non-orthogonal multiple access (NOMA) in 5G systems: Potentials and challenges," *IEEE Commun. Surveys Tuts.*, vol. 19, no. 2, pp. 721–742, 2nd Quart., 2017.
[20] M. Shirvanimoghaddam, M. Dohler, and S. J. Johnson, "Massive non-orthogonal multiple access for cellular IoT: Potentials and limitations," *IEEE Commun. Mag.*, vol. 55, no. 9, pp. 55–61, Sep. 2017.
[21] O. Kucur, G. K. Kurt, M. Z. Shakir, and I. S. Ansari, "Nonorthogonal multiple access for 5G and beyond," *Wireless Commun. Mobile Comput.*, vol. 2018, pp. 1–2, Jul. 2018.
[22] M. A. Sedaghat and R. R. Muller, "On user pairing in uplink NOMA," *IEEE Trans. Wireless Commun.*, vol. 17, no. 5, pp. 3474–3486, May. 2018.
[23] M. S. Ali, H. Tabassum, and E. Hossain, "Dynamic user clustering and power allocation for uplink and downlink non-orthogonal multiple access (NOMA) systems," *IEEE Access*, vol. 4, pp. 6325–6343, Apr. 2016.
[24] P. D. Diamantoulakis, K. N. Pappi, Z. Ding, and G. K. Karagiannidis, "Wireless-powered communications with non-orthogonal multiple access," *IEEE Trans. Wireless Commun.*, vol. 15, no. 12, pp. 8422–8436, Dec. 2016.

[25] Z. Xiao, L. Zhu, J. Choi, P. Xia, and X.-G. Xia, "Joint power allocation and beamforming for non-orthogonal multiple access (NOMA) in 5G millimeter wave communications," *IEEE Trans. Wireless Commun.*, vol. 17, no. 5, pp. 2961–2974, May. 2018.
[26] J. Guo, X. Zhou, S. Durrani, and H. Yanikomeroglu, "Design of non-orthogonal multiple access enhanced backscatter communication," *IEEE Trans. Wireless Commun.*, vol. 17, no. 10, pp. 6837–6852, Oct. 2018.
[27] G. Yang, X. Xu, and Y.-C. Liang, "Resource allocation in NOMA-enhanced backscatter communication networks for wireless powered IoT," *IEEE Wireless Commun. Lett.*, vol. 9, no. 1, pp. 117–120, Jan. 2020, doi: 10.1109/LWC.2019.2944369.
[28] G. Yang, D. Yuan, Y.-C. Liang, R. Zhang, and V. C. M. Leung, "Optimal resource allocation in full-duplex ambient backscatter communication networks for wireless-powered IoT," *IEEE Internet Things J.*, vol. 6, no. 2, pp. 2612–2625, Apr. 2019.
[29] X. Lu, D. Niyato, H. Jiang, D. I. Kim, Y. Xiao, and Z. Han, "Ambient backscatter assisted wireless powered communications," *IEEE Wireless Commun.*, vol. 25, no. 2, pp. 170–177, Apr. 2018.
[30] C. Mikeka, H. Arai, A. Georgiadis, and A. Collado, "DTV band micropower RF energy-harvesting circuit architecture and performance analysis," in *Proc. IEEE Int. Conf. RFID-Technol. Appl.*, Sep. 2011, pp. 561–567.
[31] S. Kashyap, E. Bjornson, and E. G. Larsson, "On the feasibility of wireless energy transfer using massive antenna arrays," *IEEE Trans. Wireless Commun.*, vol. 15, no. 5, pp. 3466–3480, May. 2016.
[32] G. Yang, C. K. Ho, and Y. L. Guan, "Dynamic resource allocation for multiple-antenna wireless power transfer," *IEEE Trans. Signal Process.*, vol. 62, no. 14, pp. 3565–3577, Jul. 2014.
[33] G. Yang, C. K. Ho, R. Zhang, and Y. L. Guan, "Throughput optimization for massive MIMO systems powered by wireless energy transfer," *IEEE J. Sel. Areas Commun.*, vol. 33, no. 8, pp. 1640–1650, Aug. 2015.
[34] B. Clerckx, R. Zhang, R. Schober, D. W. K. Ng, D. I. Kim, and H. V. Poor, "Fundamentals of wireless information and power transfer: From RF energy harvester models to signal and system designs," *IEEE J. Sel. Areas Commun.*, vol. 37, no. 1, pp. 4–33, Jan. 2019.
[35] G. Yang, W. P. Tay, Y. L. Guan, and Y.-C. Liang, "Optimal power allocation for diffusion-type sensor networks with wireless information and power transfer," *IEEE Access*, vol. 7, pp. 32408–32422, 2019.
[36] A. Goldsmith, "Diversity," in *Wireless Communications*. Cambridge, U.K.: Cambridge Univ. Press, 2005.
[37] M. Hong, M. Razaviyayn, Z.-Q. Luo, and J.-S. Pang, "A unified algorithmic framework for block-structured optimization involving big data: With applications in machine learning and signal processing," *IEEE Signal Process. Mag.*, vol. 33, no. 1, pp. 57–77, Jan. 2016.
[38] A. Beck, A. Ben-Tal, and L. Tetruashvili, "A sequential parametric convex approximation method with applications to nonconvex truss topology design problems," *J. Global Optim.*, vol. 47, no. 1, pp. 29–51, May. 2010.
[39] M. Grant and S. Boyd. *CVX: MATLAB Software for Disciplined Convex Programming*. Accessed: Aug. 2019. [Online]. Available: http://cvxr.com/cvx
[40] H. Gao, T. Lv, W. Wang, and N. C. Beaulieu, "Energy-efficient and secure beamforming for self-sustainable relay-aided multicast networks," *IEEE Signal Process. Lett.*, vol. 23, no. 11, pp. 1509–1513, Nov. 2016.

YATING LIAO received the B.S. degree in communication engineering from the University of Electronic Science and Technology of China, Chengdu, China, in 2019. She is currently pursuing the master's degree with the National Key Laboratory of Science and Technology on Communications, and the Center for Intelligent Networking and Communications (CINC), University of Electronic Science and Technology of China. Her current research interests include backscatter communications and the Internet of Things communications.

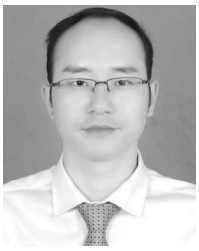

GANG YANG (Member, IEEE) received the B.Eng. and M.Eng. degrees (Hons.) in communication engineering, communication and information systems from the University of Electronic Science and Technology of China, Chengdu, China, in 2008 and 2011, respectively, and the Ph.D. degree from Nanyang Technological University, Singapore, in 2015. He was a Research Fellow with the Department of Electrical and Computer Engineering, National University of Singapore, in 2015. He is currently an Associate Professor with the National Key Laboratory of Science and Technology on Communications, and the Center for Intelligent Networking and Communications (CINC), University of Electronic Science and Technology of China. His current research interests include the Internet of Things communications, symbiotic radio-based on backscatter communications, wireless powered communications, and compressive sensing. He was a recipient of the IEEE Communications Society Transmission, Access, and Optical Systems (TAOS) Technical Committee Best Paper Award, in 2016, and the Chinese Government Award for Outstanding Self-Financed Students Abroad, in 2015. He served for the IEEE Globecom'17 as the Publicity Co-Chair.

YING-CHANG LIANG (Fellow, IEEE) was a Professor with The University of Sydney, Australia, a Principal Scientist and a Technical Advisor with the Institute for Infocomm Research, Singapore, and a Visiting Scholar with Stanford University, USA. He is currently a Professor with the University of Electronic Science and Technology of China, China, where he leads the Center for Intelligent Networking and Communications. He serves as the Deputy Director of the Artificial Intelligence Research Institute. His research interests include wireless networking and communications, cognitive radio, symbiotic networks, dynamic spectrum access, the Internet of Things, artificial intelligence, and machine learning techniques.

Dr. Liang is a Foreign Member of Academia Europaea. He has been recognized by Thomson Reuters (now Clarivate Analytics) as a Highly Cited Researcher, since 2014. He received the Prestigious Engineering Achievement Award from the Institution of Engineers, Singapore, in 2007, the Outstanding Contribution Appreciation Award from the IEEE Standards Association, in 2011, and the Recognition Award from the IEEE Communications Society Technical Committee on Cognitive Networks, in 2018. He was a recipient of numerous paper awards, including the IEEE Jack Neubauer Memorial Award, in 2014, and the IEEE Communications Society APB Outstanding Paper Award, in 2012. He was the Chair of the IEEE Communications Society Technical Committee on Cognitive Networks, and served as the TPC Chair and Executive Co-Chair for the IEEE Globecom'17. He was also an Associate Editor-in-Chief of the *World Scientific Journal on Random Matrices: Theory and Applications*. He is the Founding Editor-in-Chief of the IEEE JOURNAL ON SELECTED AREAS IN COMMUNICATIONS: COGNITIVE RADIO SERIES, and the Key Founder and the Editor-in-Chief of the IEEE TRANSACTIONS ON COGNITIVE COMMUNICATIONS AND NETWORKING. He is also serving as the Associate Editor-in-Chief for *China Communications*. He served as the Guest/Associate Editor of the IEEE TRANSACTIONS ON WIRELESS COMMUNICATIONS, the IEEE JOURNAL OF SELECTED AREAS IN COMMUNICATIONS, the *IEEE Signal Processing Magazine*, the IEEE TRANSACTIONS ON VEHICULAR TECHNOLOGY, and the IEEE TRANSACTIONS ON SIGNAL AND INFORMATION PROCESSING OVER NETWORK. He was a Distinguished Lecturer of the IEEE Communications Society and the IEEE Vehicular Technology Society.